MICROELECTRODES IN ARTIFICIAL SYNAPSES: A STUDY OF OXIDATIVE STRESS AT THE CELLULAR LEVEL

Christian Amatore [a*], Stéphane Arbault [a], Delphine Bruce [a],
Pedro de Oliveira [b], Marie Erard [a] and Monique Vuillaume [a,c]

[a] *Ecole Normale Supérieure, Département de Chimie UMR CNRS 8640 "PASTEUR"*
24, rue Lhomond, 75231 Paris Cedex 05, France
[b] *Faculté des Sciences Pharmaceutiques et Biologiques, Université René Descartes (Paris 5)*
4, avenue de l'Observatoire, 75720 Paris Cedex 06, France
[c] *Institut A. Lwoff, UPR CNRS 2169, 7 rue G. Moquet, BP 8, 94801 Villejuif, France*

Abstract

Platinized carbon microelectrodes (~ 10 μm diameter), positioned close (~ 5 μm) to the cell membrane of a human fibroblast, the ensemble constituting a semi-artificial synapse, are used to monitor events at the cellular level. A few tens of femtomoles of reactive oxygen species produced and emitted by the cell upon mechanical pricking with a glass micropipette (~ 1 μm diameter) are released into the liquid film of some hundred femtolitres comprised between the cytoplasmic membrane and the electrode surface, leading to a sudden and drastic rise in their concentrations (in the order of several micromoles). This oxidative stress-type response aims at disarming the aggressor and is thought to be shared by many (if not all) eukaryotic cells. This method allows to detect in real time and quantify the species constituting the oxidative burst cocktail: hydrogen peroxide, H_2O_2, peroxynitrite, ONO_2^-, nitrogen monoxide, NO°, and nitrite, NO_2^-. They are likely to derive ultimately from superoxide anion, $O_2^{\circ -}$, and nitrogen monoxide, NO°, synthesised by NADPH oxidase and NO synthase enzyme systems, respectively. By placing the microelectrode at different positions about the injured area of the cell membrane, it was concluded that the signals correspond to a spherical diffusion of the emitted electroactive species from a point-source.

Keywords: amperometry, microelectrodes, oxidative stress, peroxynitrite, single cell.

Portugaliae Electrochimica Acta, 19 (2001) 145-163

Introduction

Aerobic cells are known to actively synthesise reactive oxygen and nitrogen species, ROS and RNS, under the influence of stimuli like chemical messengers, xenobiotics, infectious entities (*eg.* viruses and bacteria) and physical agents (*eg.* high-energy radiation, mechanical intrusion). The levels of these potentially hazardous oxidants are kept under control by reducing substances such as vitamins and glutathione, and by enzymes like catalase and superoxide dismutase, SOD. However, in some situations the sudden production of ROS and RNS in quantities well above the physiological levels may drastically upset this delicate balance, giving rise to a metabolic condition, in which there is a surplus of oxidising species, known as oxidative stress [1-3].

Oxidative stress is thought to be involved in the onset of several human pathologies, namely arthritis, inflammation, ageing, carcinogenesis, Alzheimer disease and AIDS [1,4-7], and is known to induce apoptosis [8]. Even if the long time effects of oxidative blasts have been studied based upon the analysis of metabolites and metabolic pathways, the very primary process at the cellular level, involving the release of minute amounts of quantity (attomoles to femtomoles) in less than a few seconds, and being therefore an analytical challenge [9-11], has seldom been analysed in detail [12]. The strategy followed in this work was inspired by the cunning information transmission at the neuronal synapse: a tiny amount of neurotransmitter (a few attomoles) is released into the synaptic volume ($\approx 1\ \mu m^3$), resulting in a concentration rise of a few millimolar, easily detected by the receptor neurone. If the latter is replaced by an electrode positioned close enough (a few microns) to an emitting cell, the ensemble constitutes a semi-artificial synapse [9,13], fig 1. However, electrodes pick up noise through their capacitances, *ie.* their overall surface areas, and for an adequate signal-to-noise (S/N) ratio to be obtained (still assuming a sudden concentration rise of a few millimolar in the synapse), microelectrodes (10-20 μm diameter and whose active surfaces match in size the cell membrane area facing them) were used, since the analytical information derived from the Faraday current ultimately originating in the living cell was left untouched, while the capacitive noise was drastically reduced.

Superoxide, $O_2^{\bullet-}$, is constantly produced via a side route of the oxido-reductases that oxidise C-H bonds, and which constitutes 6-8% of the oxygen metabolism [14]. Also, many cells lines, especially those that are implicated the constitutive immune response, are known to actively synthesise $O_2^{\bullet-}$ when stimulated [1,16]. It quickly disproportionates to hydrogen peroxide, H_2O_2, and molecular oxygen, O_2, a process catalysed by SOD in aerobic cells [1,14]. H_2O_2 may be regarded as a cytotoxic substance, since it has a life time long enough to be able to diffuse to any cellular compartment, where it can give rise to hydroxyl radicals, $OH^{\bullet}$, through the Fenton reaction. The latter species, being a potent hydrogen atom acceptor, may induce several degenerative processes, namely the peroxidation of biological membranes [1,14]. In living cells, H_2O_2 is metabolised by catalase, but this enzyme is inhibited by its own substrate when the latter reaches concentrations larger than the physiological ones (*ie.* beyond the nanomolar range), other scavengers requiring at least half an hour to become operative [1,15]. Other species possibly involved in an oxidative stress response are nitrogen monoxide, $NO^{\bullet}$, produced by NO synthases (a group of enzymes that require O_2 to be operative) [1] and peroxynitrite, ONO_2^-, the outcome of the coupling between $O_2^{\bullet-}$ and $NO^{\bullet}$ at a rate close to the diffusion limit [17], according to:

$$O_2^{\bullet-} + NO^{\bullet} \rightarrow ONO_2^- \ (k \approx 2x10^{10}\ M^{-1}s^{-1}).$$

This work aimed at identifying the chemical species covered by the acronyms "ROS" and "RNS" and at monitoring their emission kinetics in oxidative stress responses triggered in human fibroblasts (used as models of skin carcinogenesis [13]) resorting to an electrochemical approach.

Results and Discussion

An oxidative stress response was triggered in human fibroblasts by pricking the cytoplasmic membrane with a sealed glass micropipette ($\approx 1\ \mu m$ diameter) [18], fig 1.

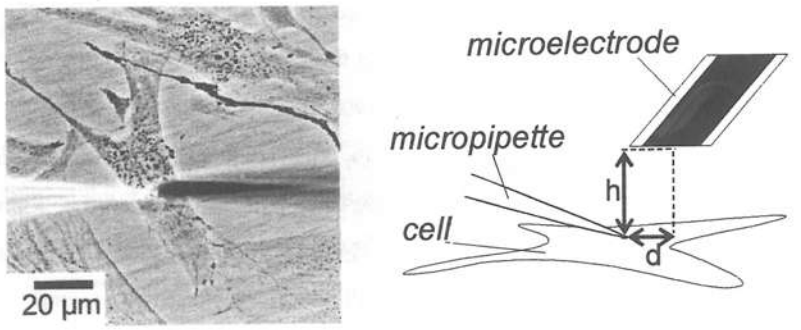

Fig 1 - Snapshot (left) and schematic representation (right) of a semi-artificial synaptic configuration consisting of a human fibroblast (on the bottom of a Petri dish) with an ultramicroelectrode positioned above it. A micropipette used to induce the oxidative burst is inserted between them.

A microelectrode poised at appropriate constant potentials and placed a few micrometers above the injured area [18] detects the flow of electroactive species emitted by the cell in the form of a Faradaic current, fig 2. Each electrode consists of carbon disk rendered more sensitive to small molecules through platinization. This markedly increases the electrode capacitance, ruling out the use of transient methods like fast cyclic voltammetry (*ca.* 50-100 Vs^{-1}). Slow potential scan rates (< 1 Vs^{-1}) are also excluded, since the scan durations would roughly match the signal half-widths (fig 2), resulting in very distorted voltammograms [19]. The electrochemical analysis had, then, to rely on the collection of independent amperograms, each obtained at different potentials on different cells [20]. This leads to another problem: cell variability. Indeed, all fibroblasts on a Petri dish are not expected to be exactly at the same metabolic stage, and the intensity of the responses varies when they are mechanically stimulated. This drawback may be skirted by collecting enough curves at each potential so that the resulting average amperogram is affected by a small standard deviation (*viz.* within ±5% for a 70% confidence level, or ±10% for a 95% confidence level). Statistically meaningful data were obtained with 25 to 40 individual measurements per potential (fig 2).

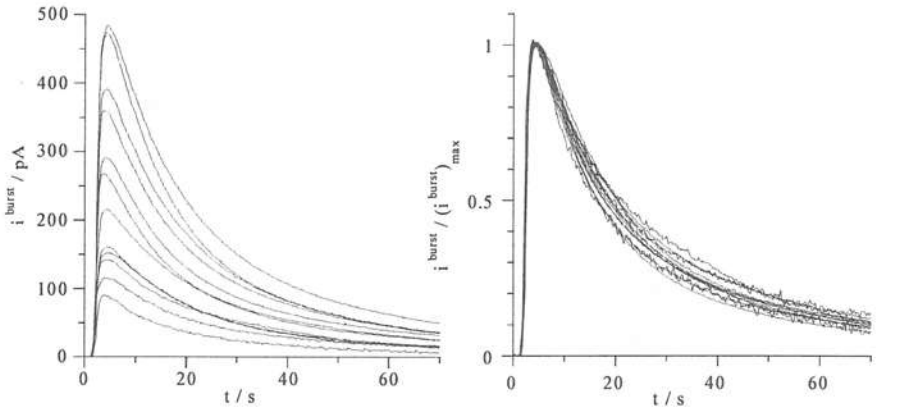

Fig 2 - Left: time dependence of the anodic currents monitored at different potentials after the stimulation of a human fibroblast by the micropipette, when the electrode (10 µm radius) is positioned at h = 5 µm right above the cell (d = 0 µm). From bottom to top: the electrode potential, E, was varied from 300 to 850 mV *vs.* SSCE by steps of 50 mV. Each curve represents the average of 25 to 40 individual events. Right: normalization of the traces relative to their individual maximum current value.

Fig 2 shows that the Faradaic current, i, increases with the applied potential, hinting at the involvement of several electroactive species [21]. The response kinetics does not correspond to simple diffusion of electroactive species from the cell, but reflects an active production process [13]. Also, since the normalised curves roughly coincide, the burst revealing a single flux temporal flow, it is licit to think that the species probably have sizes close to each other and interact with the solvent in a similar way. Last but not least, the current maximum, $(i^{burst})_{max}$, is reached after a time lag, t_{max}, which is independent of the electrode-cell distance (provided this remains below 10 µm), and larger than the microelectrode response time (a few milliseconds) [22]. For a vertical separation of 5 µm and $D = 2x10^{-5}$ cm^2s^{-1}, and assuming that $D = h^2/t_{max}$, the diffusional flight is estimated at 12 ms, a value smaller than the characteristic time of the oxidative burst response, implying that the curves reflect the kinetics of release of small species into the extracellular fluid without any significant distortion by diffusion or by the electrode response time [19].

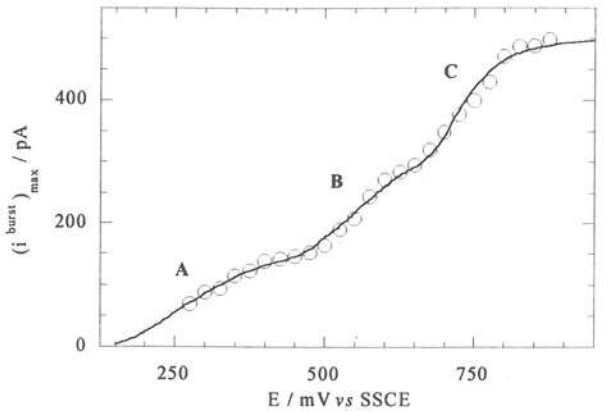

Fig 3 - Symbols: experimental variations of the current maxima, $(i^{burst})_{max}$, of the curves shown in fig 2 with the electrode potential, E. Curve: predicted voltammogram for a virtual solution of 1.4 μM H_2O_2, 1.7 μM ONO_2^-, 19 μM NO° and 4 μM NO_2^-.

The symbols in fig 3, obtained by plotting $(i^{burst})_{max}$ of the amperograms in fig 2 as a function of the potential, E, reveal the presence of three oxidation waves (A, B and C) with half-wave potentials, $E_{1/2}$ (±5 mV), at 290 (A), 555 (B) and 730 (C) mV *vs.* SSCE, which require the involvement of at least three species. Waves B and C correspond to the oxidation of NO° (one-electron) and nitrite, NO_2^- (two-electron), respectively, as revealed by the close match with authentic steady state voltammograms obtained *in vitro* with the same microelectrodes in PBS solutions of these two species (fig 4): the half-wave potentials coincide, as do the kinetics of the charge transfer [23,24].

Assigning a species to wave A is not straightforward: among the three most plausible candidates, $O_2^{\bullet-}$, H_2O_2 and ONO_2^-, the first may be excluded bearing in mind its near diffusion limit coupling with NO° yielding ONO_2^- [17], the second has $E_{1/2}$ = 250 mV *vs.* SSCE (two-electron), and the direct electrochemical behaviour of the third has recently been investigated [25].

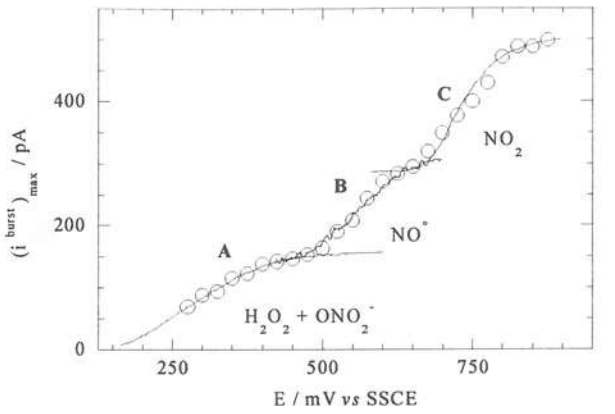

Fig 4 - Comparison of the experimental data determined between 275 and 875 mV *vs.* SSCE (solid symbols) to the *in vitro* voltammograms of NO° (19 μM) and NO_2^- (4 μM) under identical conditions. The assignment of H_2O_2 and ONO_2^- to wave A is explained below.

Peroxynitrite is a short-lived species at physiological conditions ($t_{1/2} \approx 1$ s at T = 25°C and pH = 7.4) since it decays to nitrite and nitrate ions via the intermediate formation of its conjugated acid ONO_2H (pK_a = 6.8) [17]. Its electrochemical signature had to be obtained in alkaline solutions, where $t_{1/2}$ ranges from a few minutes at pH = 9 to over an hour at pH = 12. Note that this problem is circumvented *in vivo* due to the diffusion time from the cell to the electrode surface of a few milliseconds, during which a possible loss of no more than 10% of the amount produced could ensue [19,25].

During the reaction time (*ca.*≈ 1 hour) required for the synthesis of peroxynitrite, aliquots of the reaction mixture were collected and tested both electrochemically with platinized carbon fibre microelectrodes and spectrophotometrically. The magnitude of the plateau currents of the waves O_I and O_{II} increased with time (fig 5a) following for wave O_I a strict correlation with the absorbance of the respective solution measured at λ = 302 nm (fig 5b), characteristic of the peroxynitrite anion [26]. The spontaneous decomposition kinetics of peroxynitrite solutions at several pH values were analysed by both methods. A good correlation between the decay rates of the plateau current of wave O_I and that of the absorbance at 302 nm was again obtained (fig 5c). The first-order kinetics rate constants determined from wave O_I decay are close to those reported in the literature for peroxynitrite: i.e., $k = 8 \times 10^{-5}$ s^{-1} (pH = 12), to be

compared to $k = 1x10^{-5}$ s^{-1} (as calculated at pH = 12 in ref [27]) or $k = 8x10^{-5}$ s^{-1} (pH = 11) [28]. Conversely, wave O_{II} remained virtually unchanged after completion of the synthesis, and closely matched that obtained with a solution containing NO_2^-. These facts strongly suggest that wave O_I corresponds to ONO_2^-, while wave O_{II} is due to NO_2^-. The latter will not be further discussed here.

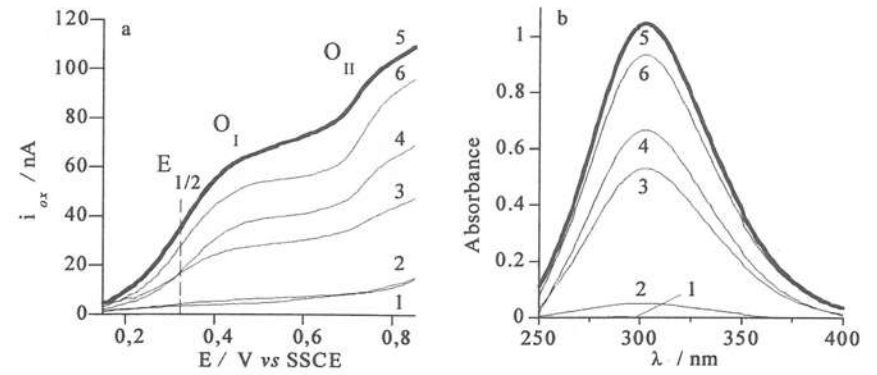

Fig 5 - Peroxynitrite synthesis during the ozonation of an azide solution (pH = 12) followed by: (a) steady state electrochemistry (20 mVs^{-1}) or (b) spectrophotometry (λ = 302 nm). Measurements were taken at 0, 10, 30, 50, 55 (bold curves, current maxima and absorbance) and 60 minutes after the beginning of ozonation. O_I ($E_{1/2}$ = 0.350 V *vs.* SSCE) and O_{II} correspond to the oxidation of ONO_2^- and NO_2^-, respectively, at platinized carbon-fibre microelectrodes (10 µm diameter). (c) Correlation (5 data points, 3 experiments for each point) between the decomposition rate constants of ONO_2^- solutions followed by UV-spectrophotometry ($\log k_{uv}$) and electrochemistry ($\log k_{elec}$) at several pH values (from 8.7 up to 10.2 from right to left). A dashed line with unity slope is shown to help the comparison. (d) Evidence for the absence of any correlation between $E_{1/2}$ of wave O_I and the pH over the range $8.8 \leq pH \leq 10.2$. All electrochemical experiments shown in this figure were carried out with platinized carbon fibre microelectrodes (10 µm diameter) in phosphate buffer solutions of ONO_2^-.

The pH dependence of $E_{1/2}$ of wave O_I is shown in fig 5d. The pH was confined to the basic side of the scale, since the half-life of ONO_2H is too short for it to be detected under the experimental conditions employed here at neutral pH. $E_{1/2}$ remains close to 0.350 ± 0.020 V *vs.* SSCE in the range $8.8 \leq pH \leq 10.2$ at platinized carbon-fibre microelectrodes despite a certain scattering of the data. This scattering is presumably due to uncontrolled alterations of the platinized surfaces in these basic media [29,30], since the $E_{1/2}$ value is controlled by the kinetics of the initial transfer and is thus dependent on the electrode surface properties [25,31]. The absence of any systematic dependence of $E_{1/2}$ for wave O_I with the pH confirms that the electrochemical process does not involve protons. Since $pH > pK_a = 6.8$, this implies that wave O_I represents the direct oxidation of ONO_2^- (and not the conjugate acid, ONO_2H, through a CE sequence) into its radical $ONO_2^\bullet$. Furthermore, since the maximum oxidation degree of nitrogen is +VI, as in $ONO_2^\bullet$ [27], this implies that the primary redox reaction is necessarily a one-electron process giving rise to $ONO_2^\bullet$ as the primary intermediate.

Wave A in fig 3 is rather sluggish and asymmetric [19], and its $E_{1/2}$ = 290 mV falls between those of H_2O_2 and ONO_2^-, at 250 mV and 350 mV *vs.* SSCE, respectively, suggesting that it may be a convolution resulting from the simultaneous presence of H_2O_2 and ONO_2^-. To test for this hypothesis, the current, i^{burst}, measured at each potential was considered as the sum of the individual currents due to each species, $i^{H_2O_2}$ and $i^{ONO_2^-}$, determined under the same conditions for the oxidation of authentic solutions of H_2O_2 (1.5 µM) and ONO_2^- (1.5 µM) according to:

$$i^{burst} = f \times [\varepsilon \times i^{H_2O_2} + (1 - \varepsilon) \times i^{ONO_2^-}],$$

where ε is a weighting parameter and f a scaling factor. The treatment of the nine data points in fig 6 afforded f = 2.1 and ε = 0.45, giving a very good correlation between the experimental and the predicted currents (i^{pred} / pA = 1.005 × $(i^{burst})_{max}$ / pA - 0.485; correlation coefficient 0.994).

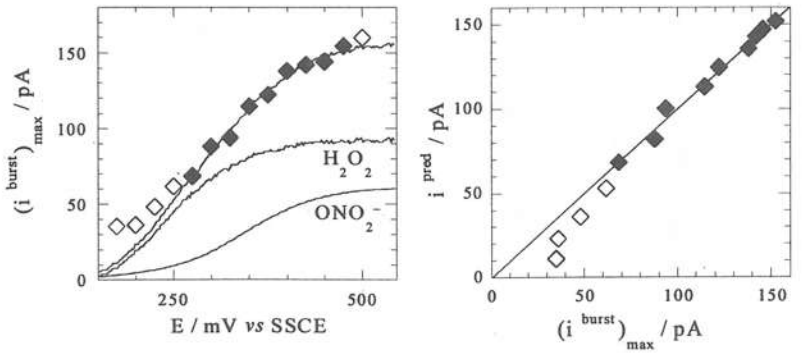

Fig 6 - Reconstructed voltammogram (symbols) from measurements obtained from 275 to 475 mV *vs.* SSCE (h = 5 μm; 10 μm radius electrode). Left: comparison between the experimental data (solid symbols) and the *in vitro* voltammograms obtained under identical conditions for H_2O_2, (1.5 μM) or ONO_2^- (1.5 μM). The unlabelled solid curve is that predicted for a mixture of H_2O_2, 1.4 μM, and ONO_2^-, 1.7 μM, under identical conditions. Right: correlation between experimental (symbols) and predicted voltammograms (i^{pred}/pA = 1.005 × $(i^{burst})_{max}$/pA - 0.485; correlation coefficient 0.994). The experimental data points obtained below 275 or above 475 mV *vs.* SSCE are indicated (open symbols) but were not considered in the fitting procedure to ensure that the data points used are not contaminated by the residual oxygen reduction [21] or by NO oxidation current.

This reasoning may be applied to the whole experimental voltammogram in fig 3, leading to a reconstructed curve by the simple addition of the voltammograms obtained for each species and taking into account their concentrations, *ie.* after an adequate scaling along the current axis. The oxidative burst corresponds, then, at the level of the electrode surface, to a mixture that, in vitro, would be equivalent to 1.4 μM H_2O_2, 1.7 μM ONO_2^-, 19 μM NO° and 4 μM NO_2^-, all ultimately deriving from $O_2^{\circ-}$ and NO°.

NADPH oxidases and NO synthases, two enzyme systems know to exist both in the cytosol and in the membranes of cells, are responsible for the production of $O_2^{\circ-}$ and NO°, respectively [1,32]. This raises another question, concerning the origin of the oxidative burst: is the burst cocktail emission a phenomenon extended throughout the whole membrane surface, or is it localised at the injured area? In the first case, a planar

diffusion of the electroactive species from the membrane would dominate, meaning that the current magnitude would depend just on the vertical distance, h, to the cell membrane as a whole, while in the second situation, explained by spherical diffusion of the electroactive species from the puncture, the current would be inversely proportional to the separation between the electrode surface and the injured area, $(h^2 + d^2)^{-1/2}$ (see fig 1 for the definitions of h and d).

Fig 7(right) shows that i^{burst} linearly varies with $(h^2 + d^2)^{-1/2}$ for separations greatly exceeding the microelectrode radius, proving that the burst cocktail is released from a point-source (and therefore spherical diffusion applies), but tends to a constant value at shorter distances, which is perfectly normal when the collection efficiency virtually equals 100% [33,34]. The single point-source origin of the oxidative burst is further supported by the result shown in fig 7(left): if a glass micropipette, after having pricked the cell membrane and being withdrawn, is slithered back in the orifice so as to block it, the response markedly decreases. When the capillary is withdrawn again, the current resumes a normal decay after overshooting for a few seconds, probably due to the sudden release of species accumulated inside the fibroblast.

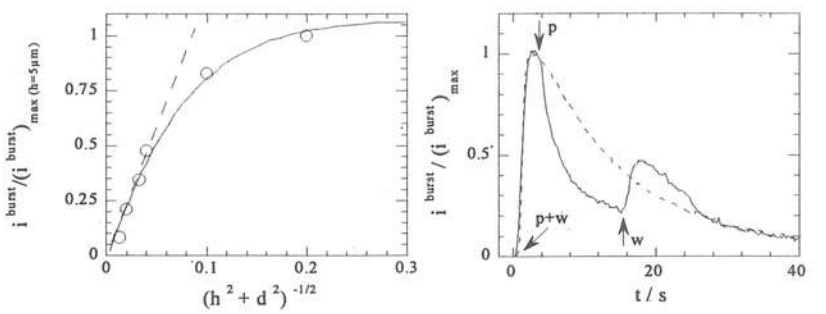

Fig 7 - Left: variations of the current collected by the electrode (450 mV *vs.* SSCE) as a function of h and d (see fig 1). Each value (open circles) is the average of at least 20 different current measurements, and has been normalized to that measured at h = 5 μm (and d = 0 μm), to indicate the variation of the collection efficiency. Right: solid curve: variations of the current detected by the electrode (560 mV *vs.* SSCE; h = 5 μm, d = 0 μm) when the micropipette pricks and is withdrawn (p + w), is pushed back (p) into the membrane hole, or withdrawn again (w); dashed curve: control (compare with fig 2).

Since when h = 5 μm (and d = 0 μm) the collection efficiency is quantitative, the current magnitudes in fig 3 do not reflect classical electrochemical steady state situations [33], but represent the quantitative collection of the molecular fluxes Φ (in mol s^{-1}) of chemicals released by the cell, converted into currents through Faraday's law by oxidation at the electrode surface [35]:

$$i^{burst} = \Sigma (n_j F \times \Phi_j)$$

where the summation encompasses all species j oxidized at the collecting ultramicroelectrode through a process involving n_j electron(s) per molecule at the potential under consideration. Applying this equation to the data contained in fig 3, and bearing in mind that the oxidation waves of NO° and ONO_2^- correspond to one-electron processes (n_j = 1), while those for H_2O_2 and NO_2^- involve two electrons (n_j = 2), the variations of the fluxes, Φ_j, with time can be determined, fig 8 [36]. The time integration of these fluxes over the whole duration of the oxidative burst affords the overall quantity of each species released. It is then deduced that an average oxidative burst corresponds to the release within less than one minute ($t_{1/2} \approx 20$ s) of a cocktail composed of H_2O_2 (15 fmol), ONO_2^- (15 fmol), NO (30 fmol) and NO_2^- (15 fmol) [19]. Applying the following equations:

$$(\Phi_{O_2^{\cdot-}})^{prod} = 2(\Phi_{H_2O_2})^{mes} + (\Phi_{ONO_2^-})^{mes} + (\Phi_{NO_2^-})^{mes}$$

$$(\Phi_{NO})^{prod} = (\Phi_{NO})^{mes} + (\Phi_{ONO_2^-})^{mes} + (\Phi_{NO_2^-})^{mes}$$

the original production fluxes $(\Phi_j)^{prod}$ for $O_2^{\cdot-}$ and NO° can be obtained, fig 8, as well as the total amounts produced during an oxidative stress burst, *viz.* 60 fmol $O_2^{\cdot-}$ and 60 fmol NO°, scheme 1.

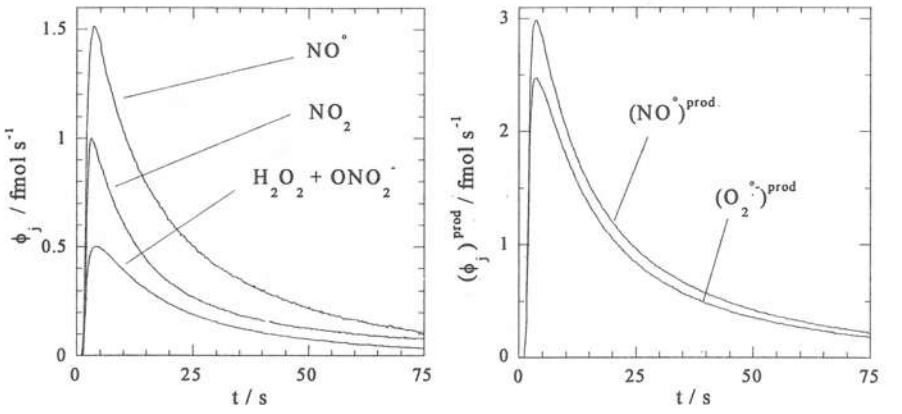

Fig 8 - Time variations of the individual fluxes determined for each species present in oxidative bursts (note that the fluxes of H_2O_2 and ONO_2^- coincide) (right), as well as those of the parent species $O_2^{\cdot-}$ and NO° (left). Each curve shown represents the average of 30 individual measurements.

Scheme 1

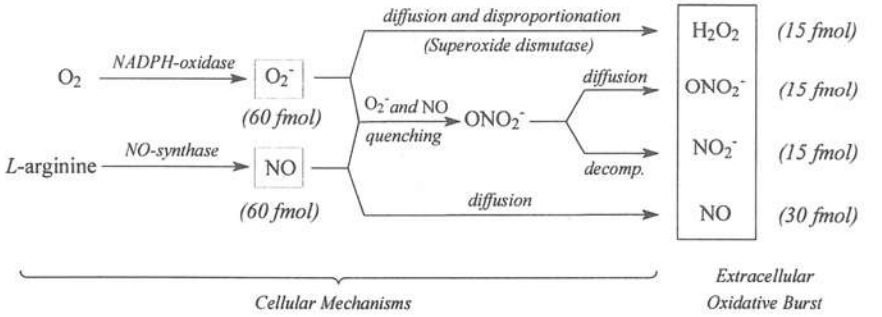

The use of inhibitors for NADPH oxidases and NO synthases has confirmed the involvement of these enzyme systems in the oxidative stress response. Indeed, N-ethylmaleimide, NEM, a denaturating inhibitor of NADPH-oxidase [37], and N^G-monomethyl-L-arginine, NMMA, a competitive inhibitor specific of NO-synthases [38], influence the response magnitude at several potentials, but more data is needed before other conclusions may be drawn.

Experimental

Single cells experiments: All the experiments have been performed at 25°C in Petri dishes placed on the stage of an inverted microscope. The electrode and micropipette were positioned with respect to the cell with two micromanipulators. All the relative details as well as those concerning the platinized carbon fiber microelectrodes construction, electrochemical apparatus, PBS solutions or cell culture and handling are identical to those reported previously [13]. The fibroblasts used in this study came from a normal human cell line (198VI) established from a skin biopsy. Cells were grown in MEM F12 medium (Gibco BRL) with fetal calf serum (10%) in an incubator (5% CO_2, 37°C). Confluent monolayers of fibroblasts were harvested by trypsination. 1000 to 2000 cells were then re-suspended in Petri dishes (3.5 cm diameter, Costar 3035) and stored in the incubator for 48 hr during which they spontaneously adhered to the Petri dish bottom. Cells were then washed three times in PBS buffer before experiments, which were only performed with isolated cells to avoid biochemical cross-talk between them during oxidative bursts.

In vitro voltammetric experiments: All reagents except peroxynitrite and nitric oxide were purchased from Sigma. Aqueous solutions were prepared with water obtained from a Millipore Milli-Q system. The *in vitro* test experiments were carried out in deareated PBS (phosphate buffer saline, 10 mM Na_2HPO_4/NaH_2PO_4, 137 mM NaCl and 2.7 mM KCl) containing either $NaNO_2$ (10 mM), ONO_2^- (6 to 20 mM), H_2O_2 (1 mM) or $NO^\bullet$ (2 mM saturated solutions). In the latter case, $NO^\bullet$ (l'Air Liquide, 99.99%) was passed through NaOH (4M) in order to scavenge any NO_x impurities and bubbled (with great caution under a fume hood) through thoroughly deaerated PBS buffer. Peroxynitrite was synthesized by ozonation of slightly alkaline azide solutions according to the procedure developed by Pryor et al [26]. Briefly, ozone was generated by passing oxygen through an ozonator (Welsbach) undergoing a silent electrical discharge (120 V). The gas stream from the ozonator, containing ~1% O_3 in oxygen, was continuously bubbled through a glass-frit in 100 mL of an aqueous solution of sodium azide (0.1-0.2 M) and NaOH (10 mM), chilled at 0°C in an ice bath. Unreacted ozone was trapped in a solution of potassium iodide (10%) in water. The peroxynitrite concentration was spectrophotometrically monitored ($\varepsilon = 1.670\ M^{-1}\ cm^{-1}$ at $\lambda = 302$ nm; Beckman DU-7400) by collecting aliquots (1 mL) of the reaction mixture at intervals of 5 to 10 min, and after dilution (8 to 12-fold) in NaOH (10 mM). The ozonation was stopped once the absorption maximum was reached (usually after 40 to 80 minutes, depending on the ozonation conditions and the initial concentration of azide). Continuing ozonation after this point would result in a progressive decomposition of peroxynitrite into nitrite. This method allows the obtaining of peroxynitrite solutions containing just traces of azide (< 0.1 mM) and virtually devoid of H_2O_2 [26]. Stock solutions of peroxynitrite (concentrations ranging from 30 to 80 mM) were stored at -20°C and used within 2 weeks, a period during which they did not decompose. During the experiments, the defrosted solutions were kept at 0°C in an ice bath to minimize the spontaneous peroxynitrite decay.

Platinized carbon-fiber microelectrodes were fabricated as previously described [13]. In the present experiments (*in vitro* and *in vivo*), the electrodeposition of platinum on the carbon microelectrodes was limited at a maximum charge of 90 μC. All potentials are referred to a saturated sodium chloride calomel electrode SSCE (Tacussel-Radiometer, France) unless otherwise indicated, since the conventional SCE reference electrode could not be used in biological systems due to possible potassium contaminations (E vs. SSCE = E vs. SCE + 5 mV, 25° C). *In vitro* voltammetric experiments were performed at 25°C in a conventional electrochemical cell, while amperometric experiments (E = +0.5 V vs. SSCE) used for the study of the peroxynitrite decomposition rate were carried out in an Eppendorf tip (500 μL). This allowed very quick mixing (just a few seconds) of the stock solution of peroxynitrite at pH = 12 with the buffer at a desired pH and allowed us to work in similar conditions as for the spectrophotometric analysis.

The UV detection of the peroxynitrite decomposition was made with the cell thermostated at 22°C. Owing to the biological relevance of peroxynitrite, biologically compatible buffers such as PBS, TRIS (Trizma base, Tris[hydroxymethyl]aminomethane, 0.1 M) and CAPS (3-[cyclohexylamino]-1-propanesulfonic acid, 0.1 M) were chosen as a function of their useful pH range (PBS:7-8; TRIS: 7-9; CAPS: 9.7-11.1) and used in the electrochemical and

spectrophotometric studies. Some experiments were carried out in phosphate solutions at pH > 9.5, which were prepared from the PBS buffer by adjusting the pH with concentrated NaOH.

Final Comments

This work demonstrates the great interest of artificial electrochemical synapses to identify and monitor the time-dependent fluxes of minute chemical quantities released by a living cell. Here, the method has been shown to lead to a very important biological information even in an extremely complex situation since several chemically interconnected species are released simultaneously by the cell, being also a challenging experimental situation because all the released molecules are difficult to characterize electrochemically due to the intrinsic sluggishness of their oxidation waves and to the impossibility of using fast voltammetric techniques.

The present series of investigations on fibroblasts establishes that the oxidative bursts are much more complex than previously assumed and that they occur within an extremely short time scale after a depolarisation of the cell membrane. They consist of a complex and concentrated cocktail of several important biological effectors: H_2O_2, ONO_2^- and $NO^\bullet$, as well as of NO_2^- as a result of ONO_2^- decomposition at physiological pH under the un-physiological concentrated conditions which prevail during oxidative blasts. All these four species result from the tandem production of $O_2^{\bullet-}$ and $NO^\bullet$ in almost equimolar amounts by two distinct enzymatic systems, NADPH oxidases and NO synthases, presumably located in different cellular compartments.

Acknowledgements

This work was supported in part by CNRS (UMR 8640 "PASTEUR"), Ecole Normale Supérieure and the French Ministry of Research (MENESR). P.d.O. thanks CNRS for a research fellowship. D.B. and M.E. thank MENESR for their PhD grants. Dr. A. Sarasin (UPR CNRS 2169, Villejuif, France) is cordially thanked for providing the cell cultures used in this study.

References

[1] B. Halliwell and J. M. C. Gutteridge, *Free Radicals in Biology and Medecine, Third edition*, Oxford University Press, Oxford (1999).

[2] H. Sies, *Angew. Chem., Int. Ed. Engl. 25* (1986) 1058.

[3] K. J. A. Davies and F. Ursini, *The Oxygen Paradox*, CLEUP University Press, Padova (1995).

[4] M.L. Gougeon, R. Olivier, S. Garcia, D. Guetard, T. Dragic, C. Dauguet and L. Montagnier, *C.R. Acad. Sci. Paris* 312 (1991) 529.

[5] L. Meyaard, S.A. Otto, R.R. Jonker, M.J. Mijnster, R. Keet and F. Miedema, *Science* 257 (1992) 217.

[6] M.L. Gougeon, *Cell Death Differ.* 2 (1995) 1.

[7] A. Lachgar, N. Sojic, S. Arbault, D. Bruce, A. Sarasin, C. Amatore, B. Bizzini, D. Zagury and M. Vuillaume, *J. Virology* 73 (1999) 1447.

[8] J.F. Torres-Roca, H. Lecoeur, C. Amatore, and M.L. Gougeon, *Cell Death Differ.* 2 (1995) 309.

[9] C. Amatore, C.R. Acad. Sci. Paris, Ser. II b, 323 (1996) 757.

[10] R.M. Wightman, P. Runnels and K. Troyer, *Anal. Chim. Acta* 400 (1999) 5.

[11] C. Amatore, Y. Bouret, E.R. Travis and R.M. Wightman, *Angew. Chem. Int. Ed. Eng.* 39 (2000) 1952.

[12] H.A.O. Hill, D.G. Tew and N.J. Walton, *FEBS Lett.* 191 (1985) 257.

[13] S. Arbault, P. Pantano, J.A. Jankowski, M. Vuillaume and C. Amatore, *Anal. Chem.* 67 (1995) 3382.

[14] *Molecular Biology of Free Radical Scavenging Systems*, ed. J.S. Scandalios, Cold Spring Harbor Press, Cold Spring Harbor (1992).

[15] W. Löntz, A. Sirsjö, W. Liu, M. Lindberg, O. Rollman and H. Törmä, *Free Rad. Biol. Med.* 18 (1995) 349.

[16] B. Meier, A. Jesaitis, A. Emmendorffer, J. Roesler and M.T. Quinn, *Biochem. J.* 289 (1993) 481.

[17] R. Kissner, T. Nauser, P. Brugnon, P.G. Lye and W.H. Koppenol, *Chem. Res. Toxicol.* 10 (1997) 1285.

[18] The relative positions of the glass capillary and the microelectrode are controlled by two independent micromanipulators (accuracy ≈ 1 µm). Their alignment is carried out under an inverted optical microscope.

[19] C. Amatore, S. Arbault, D. Bruce, P. De Oliveira, M. Erard, N. Sojic and M. Vuillaume, *Analusis* 28(6), (2000) 506.

[20] Each cell was pricked just once, and two successive curves were obtained with cells at least 50 µm apart in order to prevent cross talking.

[21] The PBS buffer in which the measurements are done necessarily has dissolved O_2 in equilibrium with the surrounding atmosphere. Its concentration is 0.24 mM, and excludes any experiments on the cathodic side of the potential scale. Indeed, the applied potential was kept above 250 mV *vs.* SSCE in order to prevent the reduction of O_2 from taking place, which might deplete the fibroblast in this vital substance (which is required for the oxidative stress response to occur), but also blast the cell with H_2O_2 produced at the electrode surface.

[22] The slope of the linear dependences of t_{max} and of the half-time width, $t_{½}$, on the square of the electrode-cell distance (for separations larger than 10 µm) lead to an average diffusion coefficient, D, of 2 x 10^{-5} cm^2s^{-1}, compatible with small species like H_2O_2, but ruling out the involvement of larger molecules like proteins, whose D is at least an order of magnitude smaller.

[23] F. Pariente, J.L. Alonso and H.D. Abruña, *J.Electroanal. Chem.* 379 (1994) 191.

[24] A.D. McGill, Y. Yang, J. Wang, L. Echegoyen and P.G. Wang, *Meth. Enzymol.* 301 (1999) 235.

[25] C. Amatore, S. Arbault, D. Bruce, P. de Oliveira, M. Erard and M. Vuillaume, *submitted.*

[26] W. A. Pryor, R. Cueto, X. Jin, W. H. Koppenol, M. Ngu-Schwemlein, G. L. Squadrito, P. L. Uppu and R. M. Uppu, *Free Radical Biol. Med. 18*(1) (1995) 75.

[27] W. H. Koppenol, J. J. Moreno, W. A. Pryor, H. Ischiropoulos, J. S. Beckman, *Chem. Res. Toxicol.* 5 (1992) 834.

[28] S. Pfeiffer, A. C. F. Gorren, K. Schimdt, E. R. Werner, B. Hansert, D. S. Bohle, B. Mayer, *J. Biol. Chem.* 272(6) (1997) 3465.

[29] C. Amatore, S. Arbault, D. Bruce, P. De Oliveira, M. Erard and M. Vuillaume, *Faraday Discuss.* 116 (2000) 319.

[29] S. B. Hall, E. A. Khudaish and A. L. Hart, *Electro. Acta* 43(5-6) (1998) 579.

[30] S. B. Hall, E. A. Khudaish and A. L. Hart, *Electro. Acta* 43(14-15) (1998) 2015.

[31] Note that the platinized electrode surfaces were checked to be stable at neutral pH when testing for H_2O_2, so this poor accuracy could not affect the results obtained *in vivo*.

[32] J.M. Robinson and J.A. Badwey, *Histochem.* 103 (1995) 163.

[33] C. Amatore, in *Physical Electrochemistry: Principles, Methods and Applications*, ed. I. Rubinstein, Dekker, New York (1995) pp.131-208.

[34] T.J. Schroeder, J.A. Jankowski, K.T. Kawagoe, R.M. Wightman, C. Lefrou and C. Amatore, *Anal. Chem* 64 (1992) 3077.

[35] C. Amatore, Y. Bouret, E.R. Travis and R.M. Wightman, *Biochim.* 82 (2000) 481.

[36] Provided it is large enough to allow for 100% collection efficiency, the diffusion coefficient plays no role in the equation. This is an extremely important notion, since the intensity and time-dependence of each flux Φ_j may be directly reconstructed from the current traces in fig 3 without knowing *a priori* the diffusion coefficients and the local concentration gradients [33].

[37] V. Le Cabec and E. Maridonneau-Parini, *J. Biol. Chem.* 270 (1995) 10631.

[38] R. Wang, A. Ghahary, Y.J. Shem, P.G. Scott and E.E. Tredget, *J. Invest. Dermatol.* 106 (1996) 419.